DOI: 10.15480/882.9328

Eighth International Symposium on Marine Propulsors
smp'24, Berlin, Germany, March 2024

Experimental investigation on the flow and deformation fields of an elastic propeller

Luca Savio[1,2], Yngve Jenssen[1], Pierre-Yves Henry[1],Giovanni Franzosi[3]

[1]SINTEF Ocean, Trondheim, Norway
[2]Department of Marine Technology, Norwegian University of Science and Technology (NTNU), Trondheim, Norway
[3]DITEN, University of Genoa (UNIGE), Genova, Italy

ABSTRACT

The hydrodynamic and structural behavior of a flexible isotropic model propeller is the subject of the present work. The propulsive performances of the propeller, the flow field in its wake and the deformation of one blade have been measured in the cavitation tunnel at SINTEF Ocean. The flow field was measured by Stereo Particle Image Velocimetry (S-PIV), while the deformations by Digital Image Correlation (DIC). The propeller was built in epoxy resin by means of casting starting from an aluminum propeller, of which one blade was used to make the mold. The aluminium propeller blades in this study have then been used as a reference propeller whose geometry, at least in model scale, could be considered to be altered to a negligible extent by the intrinsic elasticity of the material. The paper describes the experimental setup, the uncertainty in the measurements and presents the main results from the comparison of the epoxy and aluminum propellers. Previously published data on these propellers showed that the effect of flexibility could be observed on the curves of the thrust and torque coefficients both in experiments and in numerical simulations. In this work the deformations of the blades are further quantified and their effect on the propeller wake assessed, thus allowing for a more thorough comparison between simulations and experiments. The geometry of the propeller (P1566) has been previously published along with the production methods for its resin version, open water characteristics obtained in the towing tank and numerical simulations of the hydroelastic behavior of the blades. As the interest in the elastic behavior of propeller in non-cavitating condition is a topic of renewed interest in the scientific community, all data and geometries, including the tunnel geometry, can be obtained upon request, with the aim of providing validation data for numerical simulations.

Keywords

Fluid Structure Interaction, Digital Image Correlation, Particle Image Velocimetry

1 INTRODUCTION

This paper is concerned with characterizing the time averaged fluid structure interaction of a model scale propeller that has been produced in aluminium and resin. The propeller has designation P1566 and was designed by SINTEF Ocean as an open geometry propeller that could be used for research purposes. The suffixes A and R are used to denote the aluminium and resin versions of the propeller. The significant difference in stiffness of the two versions of the propeller means that the effect of the elasticity of the propeller on its performances is measurable at laboratory scale. The open water characteristics of propellers P1566A/R and fluid structure interaction simulations have already been presented by Savio et al. (2020). In this paper the characterization of the two propellers is extended by including measurements of down-stream velocity field by Stereo Particle Image Velocimetry (S-PIV), and for the flexible propeller, blade deformation by stereo digital image correlation (S-DIC).

Stereo particle image velocimetry (S-PIV) is a well-established technique in many areas of fluid dynamics that has been successfully applied to marine propellers in the past and is commonly adopted in hydrodynamic laboratories for studying the flow behind propellers (Friedhoff et al. 2021). In Felli et al. (2006) S-PIV is used to investigate the wake of a propeller and how it correlates with the evolution of the pressure field, while in Calcagno et al. (2002), it is used to study the interaction between the ship hull and the propeller.

In this project Stereo Digital Image Correlation (S-DIC) has been used to measure the deformation of the blades of propeller P1566R. Optical measurement techniques and in particular S-DIC are becoming more commonly used in hydrodynamic laboratories and in full scale to measure the deformations of flexible propeller blades (Grasso et al. 2020, Su et. al 2020). A notable alternative is the shape sensing proposed by Harwood et al. (2016), and albeit not applied to propellers yet, it has proven to be able to capture both the change in shape of elastic wings and their vibrations in wet, ventilated and cavitating conditions as it does not require optical access to the foil. It should be noted that shape sensing can be combined with optical techniques (Harwood et al. 2020).

The effect of blade flexibility on the performances of marine propellers was discussed by Atkinson and Glover

(1988) in the context of determining the deformations of full-scale nickel aluminium bronze (NAB) blades, where they showed that large marine propellers can undergo significant deformations in the tip region. Locally, as a result of the deformations, the angles of attack of the blade sections are modified from the nominal ones. However, more commonly, the topic of propeller flexibility is linked to the use of non-metallic materials as their constitutive material. Composite propellers have been for years the subject of studies as they open room for improving the structural response of marine propellers (Young 2010). Recently, it has been reported by propeller manufacturers that alternative materials to NAB have been considered to produce also conventional propellers as the stability of the supply chain for metals has been questioned.

The ability of adapting the blade shape to a changing loading by material response is often cited as the main purpose of anisotropic composite materials (Young 2008). The main mechanism by which the self-adapting behaviour is sought is the bend-twist coupling, which can be loosely described as the amount of twist that a structure shows when bent under the action of an external loading. For structures built with composite materials, bend-twist coupling can be controlled, at least to a given extent, by adjusting the layout of the fibers that are embedded in the resin (Rokvam 2020). Being able to predict during design the amount of bend-twist coupling is crucial to the success of a project and relies on the availability of reliable software predictions. The development that software solutions have had in recent years allows for setting up with relative ease fluid structure interaction (FSI) simulations and thus promoting a wider use of flexible propellers. Along with the increased interest in flexible propellers, more experimental validation material can be found in literature, but still relatively little given the complexity involved in producing high quality flexible propellers and in measuring their behaviour beside their open water characteristics. In the spirit of providing the scientific community with more validation data, the data presented here is of public domain and can be obtained upon request. The propeller geometry and experimental setup can be obtained in CAD format, while mechanical characteristics for resin used for the flexible blades are taken from the data provided by the resin producer.

2 EXPERIEMENTAL SETUP

Propellers P1566A and P1566R have a diameter of 250mm and are made of aluminium and a casting resin epoxy respectively. Details of their production method are given in Savio (2020). The propellers were tested in SINTEF Ocean's cavitation tunnel, whose test section dimensions are 6x1.3x1.2 meters, and where the water speed can be varied from 0.85 m/s to 10 m/s. The propeller was mounted in pulling condition on a H39 dynamometer by Cussons/HRW and placed in the middle of the test section as shown in Figure 1. The dynamometer measured thrust, torque, rate of revolutions of the propeller and provided a trigger signal once per revolution for synchronizing the DIC and PIV hardware. The bulk water velocity completed the list of variables needed to define the propeller characteristic parameters and was derived from the pressure difference across the nozzle upstream the test section. To further improve the accuracy of the results, the water bulk velocity is converted to propeller advance velocity by calibrating it against Laser Doppler Velocimetry (LDV) measurements of the water speed away from the tunnel walls.

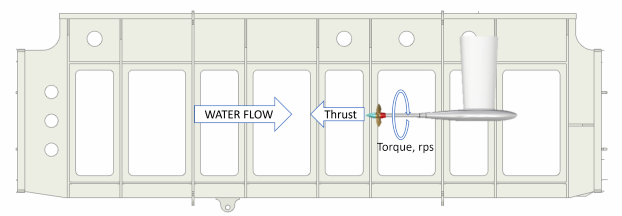

Figure 1: Propeller setup in the cavitation tunnel

The Stereo PIV flow field reconstructions (2D3C) have been carried out using a system from LaVision. The PIV plane was positioned in the wake of the propeller and spanned approximately 180 x 160 mm in streamwise and radial directions, respectively. Since the propeller has 4 blades and was pitched at pitch ratio equal to 1.1, the pitch distance was 68.75 mm, thus the field of view covered at least the passage of two blade wakes. For each of the tested conditions, 2000 double frames were acquired at a given propeller angle. Several propeller angles were tested to capture different sections of the propeller wake. The single camera resolution was 2560 x 2160 pixels, which resulted in 14 pixels per mm spatial resolution at the PIV plane, while the laser had an output energy of 200mJ and was used at 55% power. The water was seeded by polyamide particles with a size of 50 μm. The S-PIV flow field have been obtained using the commercial PIV analysis program DAVIS 10.2 from LaVision.

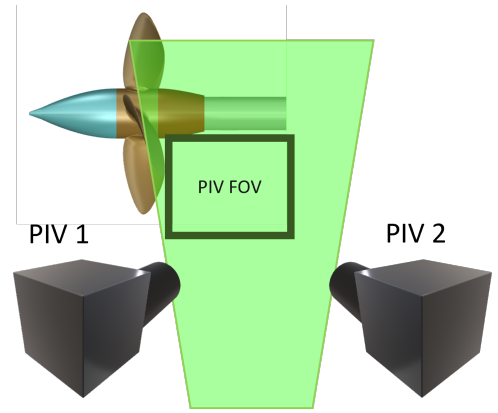

Figure 2: S-PIV setup and approximate field of view

For Stereo-DIC one blade was prepared by drawing with a marker a random dotted pattern. The blade was imaged by two high-speed cameras with a resolution of 1280 by 712 and an acquisition rate equal to 2540 frames per second. The accuracy of the system was estimated to be 0.05mm

based on the procedure proposed in Savio (2015). The high-speed cameras were started by the trigger from the propeller dynamometer every 10 seconds and a total of 25 triggers were collected per condition. The strategy of delaying the start of the recordings was adopted to ensure that the data would be recorded over a sufficiently long time span to improve statistical significance. During each recording period a few frames were collected before the next blade would cover the blade that was prepared for S-DIC. The blade root was covered by the pattern as well and was used to align the reconstructed point clouds to a point cloud that was obtained with the propeller rotating at 0.2 Hz, thus virtually without deformations. Figure 3 shows the blade prepared with the random pattern for DIC together with the coordinate system that is used to present the data. The origin of the cylindrical coordinate system is placed at the interception of the propeller shaft with the downstream face of the propeller hub. The S-DIC images have been analyzed with a code developed in-house.

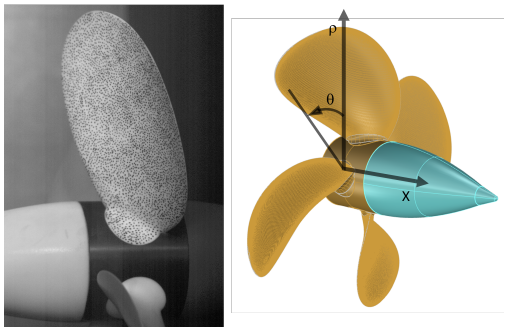

Figure 3: Blade used for S-DIC and relative coordinate system

3 RESULTS

The open water characteristics of both the aluminium and resin propellers have been evaluated at the thrust coefficients K_T equal to 0.4 and 0.2 and shown as symbols in Figure 4. The condition $K_T = 0.2$ was chosen for being representative of the design point, while the condition $K_T = 0.4$ of a highly loaded condition. The match with the data reported in Savio et al. (2020) in the towing tank (lines in Figure 4) is remarkable, especially considering that 5 years have passed since those tests and that the propellers have been re-pitched several times. The close match for the resin propeller suggests that the material has not changed its behaviour significantly. In Figure 4, the data for the propeller net thrust and torque coefficients are presented for 11 rps. The net thrust and torque are obtained from the measured data by subtracting the thrust and torque measured on a dummy hub at the same operating conditions as those tested with the full propeller.

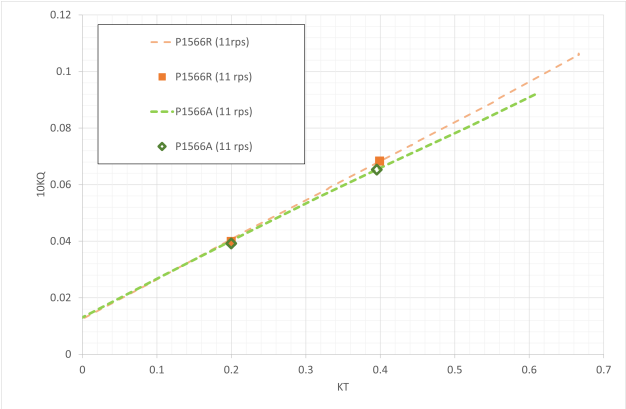

Figure 4: Net torque coefficient against net thrust coefficient for propellers P1566A and R in the towing tank in 2018 (dashed lines) and in the cavitation tunnel in 2023 (symbols)

Table 1 shows the comparison of the data collected in the cavitation tunnel and in the towing tank. The propeller characteristics repeated reasonably well, with differences below 3.5% between the two data-sets. The aluminium propeller matched more closely the data from the towing tank, while the poorest match is registered for the resin propeller at 9 rps and K_T = 0.2. No other clear pattern could be recognized in the data-set.

Table 1: Comparison of the measured net K_T and K_Q in the cavitation tunnel and towing tank

Rps [1/s]	KT	KQ CAVITATION TUNNEL	KQ TOWING TANK	Diff %
P1566R				
11	0.399	0.0683	0.0682	-0.1987
11	0.200	0.0399	0.0407	2.0844
9	0.395	0.0668	0.0670	0.2550
9	0.199	0.0394	0.0407	3.2123
P1566A				
11	0.200	0.0392	0.0401	2.2884
11	0.395	0.0653	0.0653	0.0139
9	0.201	0.0409	0.0404	-1.1528
9	0.392	0.0661	0.0650	-1.7023

The blade deformations are presented in a cylindrical coordinate system as defined in Figure 3. Of the three components of displacement, the axial DX and the tangential $\rho\delta\theta$ displacements are dominating, while the radial component $\delta\rho$ is small. Figure 5 depicts the displacement fields for P1566R at $KT = 0.4$ and 11 rps. The maximum displacements are found at the tip of the blade, and they appear to be uniformly distributed in radial and tangential directions, consistently with the approximation that the blade is deforming as a homogeneous and isotropic cantilever beam.

Figure 6 shows the total blade displacement $DS = \sqrt{DX^2 + (\rho\delta\theta)^2 + \delta\rho^2}$ averaged radially as a function of the radial location along the blade, while in Figure 7 the total average displacement is normalized by the propeller thrust.

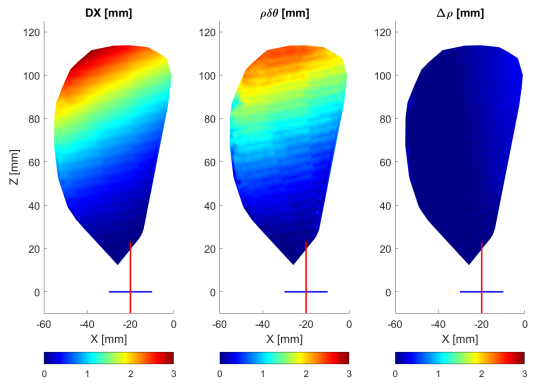

Figure 5: Blade displacements in cylindrical coordinates for the DIC blade of propeller P1566R at $KT = 0.4$ and 11 rps

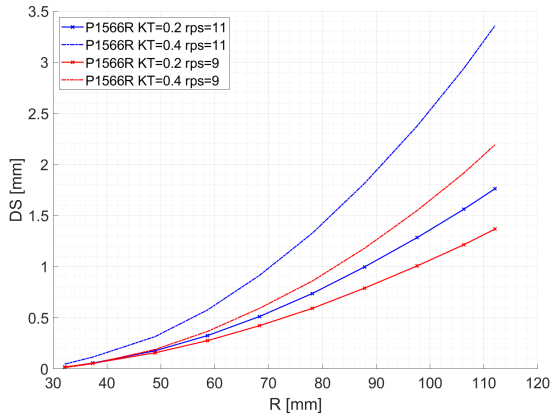

Figure 6: Radially averaged total displacement as a function of the radial location.

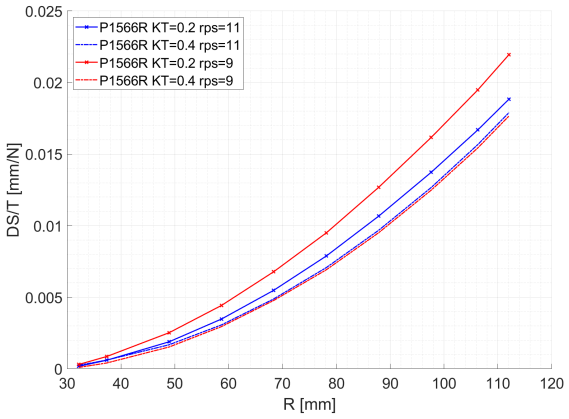

Figure 7: Radially averaged total displacement normalized by the propeller thrust as a function of the radial location.

The PIV data reveal the complicated structure of the tip vortex roll-up in the stream tube aft of the propeller as shown in Figure 8 where the turbulent shear stress is depicted.

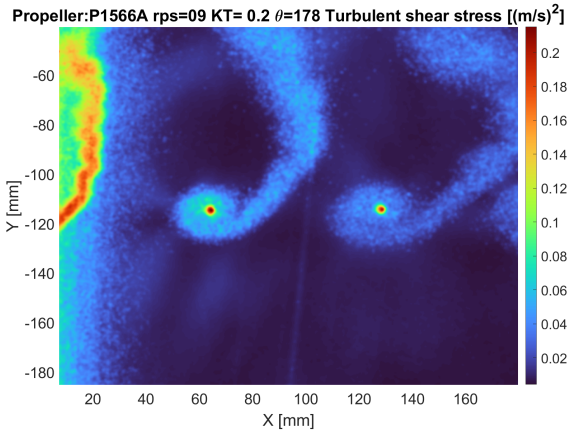

Figure 8: Turbulent shear stress in the wake of the aluminium propeller.

The identification of the vortex cores is carried out by computing the swirling intensity as suggested by Zhou et al. (1999). The vortex cores traced by the swirl intensity are clearly visible in Figure 9. The centers of the vortex cores are then identified as the local maxima of the swirling intensity.

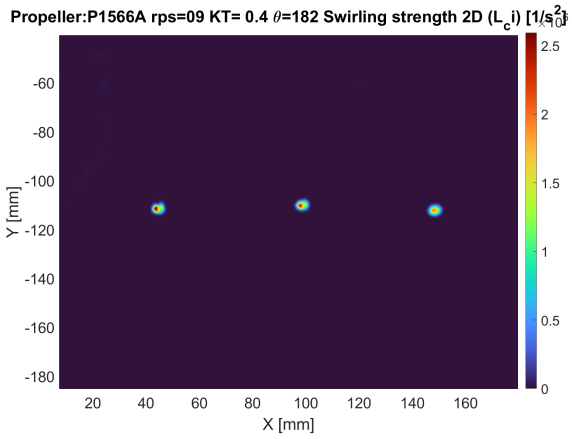

Figure 9: Swirling intensity of the tip vortexes in the aluminium propeller stream-tube.

From the location of the centers of the vortexes cores the hydrodynamic pitch angle β_i of the vortical structure shed by the propeller can be estimated as the distance between two subsequent vortexes. In Figure 10 the hydrodynamic pitch non-dimentionalized by the propeller pitch β is presented for a both the P1566A (crosses) and P1566R (circles) for 9 rps (in red) and for 11 rps (in black). The relative hydrodynamic pitch at KT = 0.2 is about 0.95 of the geometric pitch with relatively little dependency from the propeller rate of revolutions, angle and material. At KT = 0.4, the relative hydrodynamic pitch of propeller P1566R shows again little influence from the propeller angle and can be estimated to be in the proximity of 0.8, while for propeller P1566A at the angles of 178, 180 and 182 the value drops to approximately 0.725.

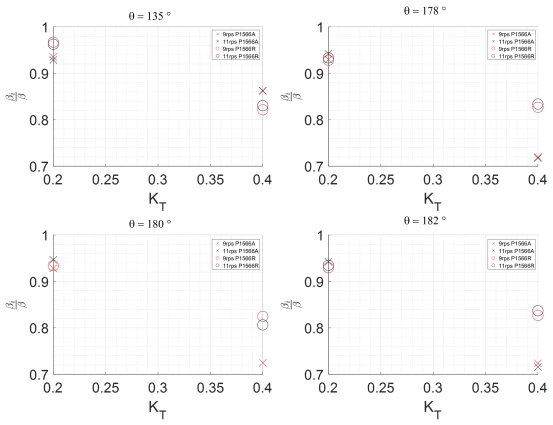

Figure 10: Hydrodynamic pitch normalized by the propeller pitch for the propeller rotation angles 135, 178, 180 and 182 degrees and for the thrust coefficients 0.2 and 0.4. Red symbols are relative to 9 rps, black to 11, while the crosses and the circles identify the aluminium and resin propeller respectively.

4 DISCUSSION

The dashed curves in Figure 4 are from the tests in the towing tank and they span the entire propulsive range of the propellers, from bollard to the advance coefficient where the propeller thrust is zero. The two curves match closely up to $KT = 0.2$, where the curves depart from each other and have different slopes. The resin propeller has a different slope than the aluminium one, thus showing the effect of the deformation of the blades on the open water characteristic. The deflection measured by S-DIC confirmed that the blades of propeller P1566R deformed during operation. Normalizing the total average displacement with the propeller thrust provides a reasonable collapse of the data. The collapse of the data is an expected result from the analogy of the blade with a cantilever beam where the load varies radially primarily as a function of the chord length. The largest deviation from a perfect collapse is found at the lowest loading which may be due to the experimental error being more significant in this case. It is worth noting that at $KT = 0.4$ the total displacement curves match notably well for both 9 and 11 rps.

However, the fact that a propeller blade can be quite well modelled from a structural point of view by a cantilever beam is the most common approximation made for the design of NAB propellers. For the design of anisotropic propellers, more detailed information on the deformation field of the blades is needed. To that end, the displacement fields are analysed in a similar way to what proposed by Savio et al. (2020) for the results from the FSI simulations. The comparison with the above mentioned numerical results can only be partial as there are three main differences between the simulations and the experiments. Firstly, the procedure to extract the blade section displacements and twist angles from the FSI simulations can only be reproduced in an approximate way from the experiments, as for practical reasons only one side of the blade is reconstructed; secondly, and more importantly, the working conditions of the propeller do not match exactly; finally, especially for the blade twist, only the trend from $x = r/R = 0.4$ can be compared as the procedure of aligning the point clouds from DIC resets both the displacements and twist at the root of the blade. Despite these limitations the comparison is presented in Figures 11 and 12 for the blade displacement and twist, respectively. In order to mitigate the shortcoming of the simulations and the experiments not being performed at the same working conditions, both the blade sections displacements and twists have been normalized by the propeller thrust, a practice that led to a reasonable collapse of the data for the experiments. The normalized displacements from the FSI simulations at J = 0.4 match to a certain extent with the experiments at KT=0.4, while a larger mismatch is observed for the FSI at J = 0.8 and experiments at KT = 0.2, which are two comparatively closer conditions in terms of blade thrust than the previous ones.

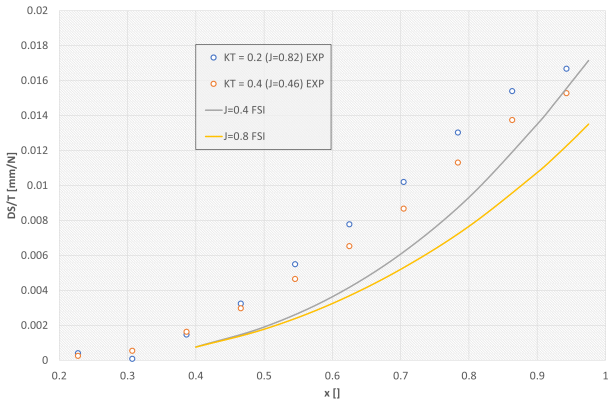

Figure 11: Comparison of the measured displacements with the FSI simulations from Savio et al. (2020).

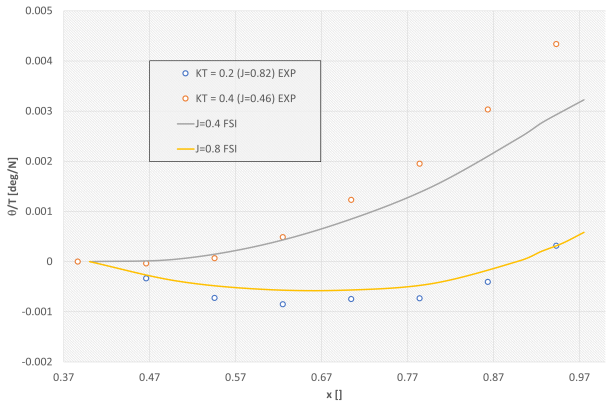

Figure 12: Comparison of the measured twist with the FSI simulations from Savio et al. (2020).

The relative twist from x = 0.4 compares closely between the experiments and the simulations as Figure 12 demonstrates. The degree of twist of a blade section can be correlated to the relative position of the neutral axis and the centre of pressure on the section, which is the driving mechanism behind bend-twist coupling. The blades in this case are homogeneous and isotropic, thus the bend- twist

coupling is entirely determined by the above-mentioned relative position of the section neutral axis and centre of pressure, but in the case of a blade manufactured in an anisotropic material, the anisotropy can be exploited to have the blade shape adapting passively to changes in load. The ability of measuring shape variations in model scale are crucial to being able to design self-adaptive propellers.

The simple analysis of the PIV data presented here did not reveal any pattern that could be correlated to the elasticity of the blades. The standard PIV processing algorithm that is used in this work does not allow for accounting for the tendency of the vortex to meander. The location of the vortex-core is obtained from the location of the averaged flow fields that have been recorded and may be different from the average of the locations of the vortex-core in the single flow fields.

5 CONCLUSIONS

The present work partially concludes the work started in Savio et al (2020) on measuring the time averaged hydroelastic response of three resin propellers that share all design parameters beside the skew distribution. Of the three geometries, only propeller P1566R was investigated in the scope of work of the tests detailed here; however, the close match with the FSI simulations and the previous results from the towing tank suggests that for homogenous isotropic propellers in uniform inflow there are reliable simulation tools of the involved physics and thus it is expected that similar results may be obtained also for the other two propellers of the series. It shall be noted that the non-metallic isotropic propellers in uniform inflow are a very idealized case that has limited practical applications. One first step towards more realistic conditions would be introducing a wake to the inflow to the propeller, in order to obtain a mechanical response from the material. The wake could be introduced by simply running the propeller with an inclined shaft to introduce an harmonic variation of the blade load. Despite the difficulties in producing model scale anisotropic propellers, it is still worth introducing anisotropy or inhomogeneities in the propeller to represent the ability to self-adapt of the blades to the changes in loading which is often cited as the ultimate goal for anisotropic propellers.

REFERENCES

Atkinson, P., & Glover, E. J. (1988). 'Propeller Hydroelastic Effects'. Propeller '88 Symposium, 1988, D031S002R011. https://doi.org/10.5957/PSS-1988-21

Calcagno G. , Di Felice F., Felli M. , Pereira F. "Propeller wake analysis behind a ship by stereo PIV" - 24th Symposium on Naval Hydrodynamics, Fukuoka . . . , 2002

Friedhoff B., Roettig F. , Wennemar K., Hoyer K., Beslac R., Hesseling C., Beck T. "Comparison of stereoscopic particle image velocimetry and volumetric particle tracking velocimetry in the wake of a ducted propeller". Ocean Engineering 234(2021)

Harwood, CM, Ward, J, Young, YL, ... (2016) Experimental investigation of the hydro-elastic response of a surface-piercing hydrofoil in multi-phase flow. 31st Symposium on . . . . researchgate.net; 2016;

Harwood CM, Felli M, Falchi M, Garg N, Ceccio SL, Young YL. (2020) 'The hydroelastic response of a surface-piercing hydrofoil in multiphase flows. Part 2. Modal parameters and generalized fluid forces.' Journal Fluid Mechanics. 2020 Feb 10;884:A3.

Grasso, N., Hallmann, R., Scholcz, T., Zondervan, G., Maljaars, P., Schouten, R. (2019).'Measurements of the hydro-elastic behaviour of flexible composite propellers in nonuniform flow at model and full scale' Sixth International Symposium on Marine Propulsors smp'19, Rome, Italy, May 2019

Savio, L. (2015) 'Measurements of the deflection of a flexible propeller blade by means of stereo imaging'. Fourth International Symposium on Marine Propulsors , smp'15 Austin, Texas, USA, June 2015

Savio, L., Sileo, L., and Kyrre Ås S. (2020). 'A Comparison of Physical and Numerical Modeling of Homogenous Isotropic Propeller Blades' Journal of Marine Science and Engineering, 8 no. 1: 21. https://doi.org/10.3390/jmse8010021

Su, Z., Pan, J., Zhang, S., Wu, S., Yu, Q., & Zhang, D. (2022). 'Characterizing dynamic deformation of marine propeller blades with stroboscopic stereo digital image correlation'. Mechanical Systems and Signal Processing, 162, 108072. https://doi.org/10.1016/j.ymssp.2021.108072

Young, Y. L. (2010). 'Dynamic hydroelastic scaling of self-adaptive composite marine rotors.' Composite Structures, 92(1), 97–106. https://doi.org/10.1016/j.compstruct.2009.07.001

Young, Y. L. (2008). Fluid–structure interaction analysis of flexible composite marine propellers. Journal of Fluids and Structures, 24(6), 799–818. https://doi.org/10.1016/j.jfluidstructs.2007.12.010

Rokvam SØ, Vedvik NP, Savio L, Echtermeyer A. Designing Composite Adaptive Propeller Blades with Passive Bend–Twist Deformation for Periodic-Load Variations Using Multiple Design Concepts. Polymers. 2023; 15(12):2749. https://doi.org/10.3390/polym15122749

Zhou, J., Adrian, R. J., Balachandar, S., & Kendall, T. M. (1999). 'Mechanisms for generating coherent packets of hairpin vortices in channel flow'. Journal of Fluid Mechanics, 387, 353–396. https://doi.org/10.1017/S002211209900467X